Article published online: 2023-01-27

Multilayer and Thin Transparent Conducting Oxide Fabrication Using RF Magnetron Sputtering on Flexible Substrates

Sanjay Kumar Swami[*,#,a]
Bidyut Barman[#,b]
Anuj Kumar[c]
Viresh Dutta[b]

[a] CSIR-National Physical Laboratory, Dr. K. S. Krishnan Marg, New Delhi 110012, India
[b] Photovoltaic Lab, Department of Energy Science and Engineering, Indian Institute of Technology Delhi, Hauz Khas, New Delhi 110016, India
[c] Department of Physics, J. C. Bose University of Science and Technology, YMCA, Faridabad, Haryana 21006, India
[*] swami.phy@gmail.com
[#] Equal contributions.

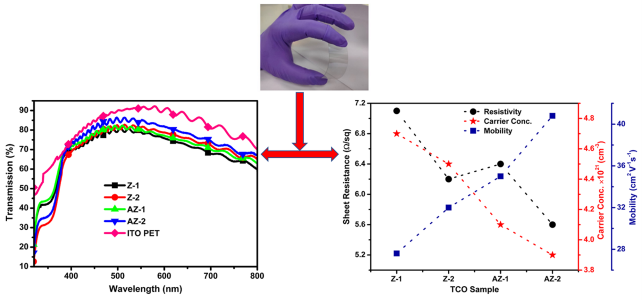

Received: 02.09.2022
Accepted after revision: 19.12.2022
DOI: 10.1055/s-0042-1757982; Art ID: OM-2022-09-0035-OA

Abstract In this work, the fabrication of multilayered transparent conductive oxides (TCOs), ZnO–Ag–ZnO (Z-TCO) and AZO–Ag–AZO (AZ-TCO), on flexible polyethylene terephthalate (PET) substrate using radio frequency (RF) magnetron sputtering is reported, with the optical and electrical properties comparable to those of the commercially available Sn-doped indium oxide (ITO) on the PET substrate. The growth of Z-TCO and AZ-TCO layers on PET (with surface roughness ~5–7 nm) shows similar surface characteristics to that on the glass substrate. The multilayered Z-TCO and AZ-TCO (total thickness ~70 nm) with 10 nm of Ag thickness (named Z-2 and AZ-2, respectively) exhibit a maximum transparency of 82.7% and 86.4%, at 515 and 498 nm, respectively. The AZ-2 layer has a lower electrical resistivity of 3.92×10^{-5} Ω cm with a lower sheet resistance of 5.6 Ω/sq, whereas for ITO on PET these values are 2.62×10^{-4} Ω cm and 14.5 Ω/sq, respectively. The AZ-2 layer also gives an excellent figure of merit (FoM) of 21.3×10^{-3} Ω^{-1}, which is better than the FoM for ITO PET (17.3×10^{-3} Ω^{-1}). Therefore, the flexible multilayer TCOs prepared using RF magnetron sputtering on PET substrates on a large area can have better optoelectronic properties than commercial flexible ITO coating and can be used in flexible optoelectronic devices.

Key words: flexible substrates, multilayered TCO, magnetron sputtering, electrical resistivity, figure of merit

Introduction

Transparent conductive oxides (TCOs) are a very significant component in wearable and mobile optoelectronic devices such as photovoltaic devices, displays, and light-emitting diodes.[1–6] Sn-doped indium oxide (ITO) is commonly used, but indium being a highly expensive material, a rapid rise in the manufacturing costs for these devices is observed.[3,4] Development of cost-effective TCOs using oxides such as TiO_2, SnO_2, ZnO, etc. is being extensively done.[7–9] Fabricating TCO films on flexible substrates like PET (polyethylene terephthalate) and PEN (polyethylene naphthalene) helps in making the devices light-weight and flexible.[10,11]

Organics materials are also used as the conductive transparent electrodes, but they have some issues such as lower electrical properties and long-term stability, which limit the growth of organic materials as transparent electrodes.[12]

For any multilayer structure to be used as TCOs, two basic conditions are to be considered: (1) the band gap of the oxide layer must be > 3.1 eV, which allows transmission of wavelengths above 400 nm to achieve more than 80% light transmittance in the visible wavelength region, and (2) the metal oxide must be degenerately doped with carrier densities of 10^{20}–10^{21} $\cdot cm^{-3}$. Metal-oxide–metal multilayer structures, e.g. ZnO–Ag–ZnO (named Z-TCO) and AZO–Ag–AZO (named AZ-TCO), achieved the combination of high conductivity due to the thin metal layer and high optical transparency due to the oxide layers, making a perfect TCO layer.[9,13,14] The benefits of using these multilayer structures as TCOs compared to a single-layered TCOs are post-deposition high-temperature processing can be avoided as one can achieve the best optoelectronic properties for the as-deposited films with optimal layer thicknesses, and the combined layer thicknesses can be lower than those for the ITO substrates with similar properties. Girtan et al. reported on multilayered TCO properties with thickness 25/8/25 nm on PET substrates with resistivity around 2×10^{-5} Ω cm and figure of merit (FoM) of 4×10^{-3} Ω^{-1}.[15] Han et al. prepared Z-TCO onto PET substrates using radio frequency (RF) and direct current (DC) sputtering,[16] with thickness 35/12/35 nm, and obtained a maximum of 75% optical transparency in the visible region of the spectrum, and 10 Ω/sq sheet

resistance. Guillén et al. investigated AZ-TCO multilayer's optical and electrical properties on a PET substrate with thickness 40/10/40 nm and reported a maximum transparency of 85% at 600 nm with an electrical resistivity of 5.6×10^{-5} Ω cm.[17] Fahland et al. reported the ITO–Ag–ITO and Nb_2O_5–Ag–Nb_2O_5 multilayer stacks with a sheet resistance of 7.5 and 7.1 Ω/sq, respectively.[18] Fabrication of highly transparent and conducting Z-TCO and AZ-TCO multilayered TCO using RF magnetron sputtering onto a glass substrate has been reported earlier.[19] The TCO layers with a thickness of around 70 nm exhibited a higher optical transparency and a lower electrical resistivity with an excellent FoM as compared to ITO glass, which makes the fabricated TCO layers suitable candidates to replace highly expensive ITO films for optoelectronic devices.[19]

In the present study, we report on Z-TCO and AZ-TCO multilayers fabricated on a flexible PET substrate. Having reported about these films on the glass substrate, it is now possible to analyze the role of the substrate on the TCO properties in order to obtain comparable properties for both the flexible and rigid substrates.

Results and Discussion

The fabricated Z-TCO and AZ-TCO films on the PET substrate with thicknesses ZnO (30 nm) + Ag (8 nm) + ZnO (30 nm); ZnO (30 nm) + Ag (10 nm) + ZnO (30 nm); AZO (30 nm) + Ag (8 nm) + AZO (30 nm); and AZO (30 nm) + Ag (10 nm) + AZO (30 nm) are named as Z-1, Z-2, AZ-1, and AZ-2, respectively. X-ray diffraction (XRD) spectra of the multilayer TCOs on PET substrates are shown in Figure 1.

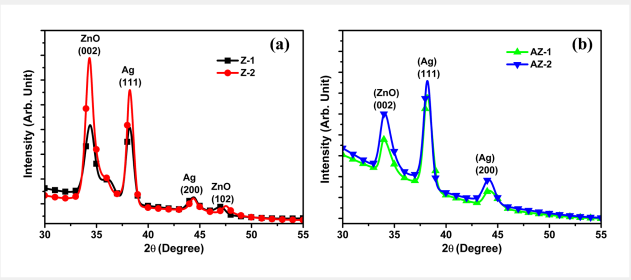

Figure 1 XRD spectra of (a) Z-1 and Z-2 and (b) AZ-1 and AZ-2 multilayer TCOs on a PET substrate.

A strong ZnO (002) peak at around 2θ = 34.3° is observed for all samples, corresponding to the hexagonal ZnO crystal structure (JCPDS (36 – 1451)). This strong ZnO (002) peak depicts the polycrystalline nature and is close to the peak for ZnO wurtzite structure at around 34.45°.[20–22] In addition, another peak corresponding to the (111) plane of Ag is observed at ~2θ = 38.18° (JCPDS (04 – 0783)).[20] Similarly, a weak ZnO (102) peak is observed at ~2θ = 47.41° for Z-TCO layers.[23,24] An Ag (200) peak also appears at ~44.36° for both Z-TCO and AZ-TCO layers.[25] Figure 1(a, b) shows a significant rise in ZnO (002) peak intensity for 10 nm Ag thickness. This indicates that with the increase of Ag layer thickness, the ZnO or AZO layer in the Z-TCO and AZ-TCO structures sustains definite crystallization improvements since the Ag layer becomes continuous at 10 nm Ag thickness. The Ag (111) peak intensity also expectedly increases for 10 nm Ag thickness, which can be due to the RF-sputtered Ag particles mixing with the top ZnO layer before forming a thin continuous layer. However, a higher ZnO (002) peak intensity was observed in the Z-TCO film as compared to the AZ-TCO film. This is due to the occupancy of the dopant Al in the ZnO lattice, the Al^{3+} ionic radius (0.54 Å) being smaller than the Zn^{2+} ionic radius (0.74 Å).

A reduction of the ZnO lattice parameter results in a lowering of the intensity of the ZnO (002) peak for AZ-TCO structures.[26–28]

The Debye–Scherrer formula was used to calculate the crystallite size (D) of zinc oxide and silver thin films for Z-TCO and AZ-TCO multilayers.[29]

$$D = \frac{0.94\,\lambda}{\beta \cos\theta} \quad (1)$$

Here, λ = 1.54 Å, θ = Bragg's diffraction angle, and β = full-width at half-maximum (FWHM).

Table 1 shows the calculated crystallite size, FWHM of the ZnO and Ag peaks using the XRD data along with the thickness of the individual layer of Z-TCO and AZ-TCO structures. The Z-TCO structures have a higher average ZnO and Ag crystallite size than those of AZ-TCO structures. The higher FWHM of AZ-TCO structures represents a wider ZnO and Ag crystal size distribution as compared to that in Z-TCO structures. Moreover, the reduced crystallinity of AZO also results in a lower particle size and broadening of ZnO and Ag particle size distribution in AZ-TCO layers.[30,31] XRD data show that the ZnO crystallite sizes for Z-1, Z-2, AZ-1, and AZ-2 layers on the PET substrate are 5.9, 8.4, 2.3, and 3.1 nm, respectively. These values are close to those on the glass substrate, which suggests that the film growth processes are similar for all the layers on either substrate.[19]

Table 1 Structural details of Z-TCO and AZ-TCO layers

TCO sample	Thickness (nm)	FWHM (2θ, deg)		Crystallite size (nm)	
		ZnO	Ag	ZnO	Ag
Z-1	ZnO (30) + Ag (8) + ZnO (30)	1.48	0.98	5.9	9.0
Z-2	ZnO (30) + Ag (10) + ZnO (30)	1.04	0.83	8.4	10.6
AZ-1	AZO (30) + Ag (8) + AZO (30)	3.80	1.24	2.3	7.1
AZ-2	AZO (30) + Ag (10) + AZO (30)	2.80	1.13	3.1	7.7

Figure 2 shows the field emission scanning electron microscopy (FE-SEM) images of Z-2 and AZ-2 films. The FE-SEM images portray non-continuous film structures with Ag particles of irregular shape and sizes, connected to each other. For 10 nm Ag thickness, the Ag particles coalesce with each other making the surface smoother and continuous.

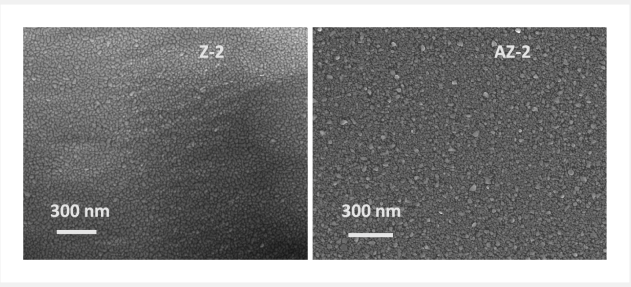

Figure 2 FE-SEM images of Z-2 and AZ-2 TCO layers.

Figure 3 shows the atomic force microscopy (AFM) images (scanning area: 2.5 µm × 2.5 µm) of Z-2 and AZ-2. The roughness values of Z-2 and AZ-2 films are 5.35 and 6.29 nm, respectively. The surface roughness (root mean square, RMS, value) of the top ZnO layer of the multilayer TCO structure on PET substrates is compared with that of ZnO surface roughness on the glass substrate, as reported in our previous article.[19] Table 2 shows that the surface roughness values of Z-TCO and AZ-TCO layers on PET substrates (~5 – 7 nm) are higher than on glass surface (roughness ~2 – 3.5 nm), even then the roughness is within the range for any device applications.

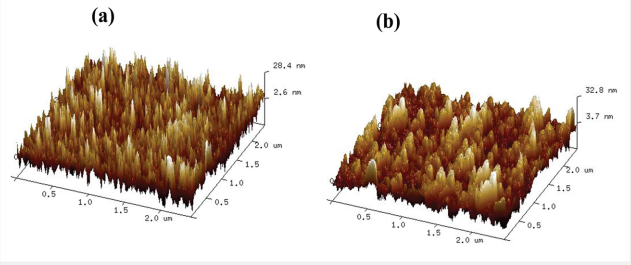

Figure 3 AFM images (a) Z-2 and (b) AZ-2 TCO layers.

Table 2 Surface roughness (RMS value) of the top oxide layer on PET and glass substrates

TCO structure	Thickness (nm)	Top layer roughness (nm)	
		PET	Glass[19]
ZnO/Ag/ZnO	30/8/30	–	2.08
ZnO/Ag/ZnO	30/10/30	5.35	1.64
AZO/Ag/AZO	30/8/30	–	3.34
AZO/Ag/AZO	30/10/30	6.29	2.89

The results obtained for Z-TCO and AZ-TCO on flexible substrates are compared with those on glass substrates as described in the earlier publication.[19] The XRD measurements reveal the hexagonal structure of the obtained films with polycrystalline nature and a strong preferential ZnO (002) peak. However, the ZnO (002) peak intensity for Z-TCO and AZ-TCO layers on the PET surface is higher than that for the glass surface. The growth behaviour of thin films on any substrate depends on various surface properties like chemical compositions and thermal and structural mismatches between the substrate and the deposited thin film. This mismatch results in the development of strain and stress in the film.[28,32,33] The developed strain and stress along with lattice constant, dislocation density, etc. of Z-TCO and AZ-TCO films using XRD spectra along the ZnO (002) orientation is calculated using the following equations:
Micro-strain[32],

$$\varepsilon = \frac{\beta}{4 \tan \theta} \tag{2}$$

where, β = FWHM in radians and θ = Bragg's angle.
Lattice constant:[33]

$$\frac{4 \sin^2 \theta}{\lambda^2} = \frac{h^2 + k^2}{a^2} + \frac{l^2}{c^2} \tag{3}$$

where h, k and l = miller indices, a and c = lattice constant, and λ = 1.54 056 Å.
Compressive stress:[27]

$$\sigma = [2C_{13} - C_{33}(C_{11} + C_{12})/C_{13}](c - c_0)/c_0 \tag{4}$$

where, c = lattice constant from the (002) plane in the XRD data, c_0 = corresponding bulk value (0.5206 nm), C_{ij} = elastic stiffness constants ($C_{11} = 2.1 \times 10^{11}$ N·m^{-2}, $C_{33} = 2.1 \times 10^{11}$ N·m^{-2}, $C_{12} = 1.2 \times 10^{11}$ N·m^{-2}, and $C_{13} = 1.05 \times 10^{11}$ N·m^{-2}). Using all these parameters, the stress is estimated from the XRD pattern by using the formulas:

$$\sigma = -4.5 \times 10^{11}(c - c_0)/c_0 \text{ Nm}^{-2} \tag{5}$$

$$\sigma = -4.5 \times 10^{2}(c - c_0)/c_0 \text{ GPa} \tag{6}$$

Table 3 shows the comparison of calculated structural parameters of Z-TCO and AZ-TCO multilayers on PET and glass substrates. The-ve sign of stress in Table 3 indicates that the stress on the films is compressive. Figure 4 shows the variation of compressive stress on Z-TCO and AZ-TCO layers for both PET and glass substrates, with the compressive stress on the glass substrates higher than that on PET substrates.

The higher compressive stress on glass substrates may be due to the amorphous nature of the glass substrate.[34] Again, compressive stress on AZ-1 and AZ-2 layers is higher than

Table 3 Structural parameters of Z-TCO and AZ-TCO layers on PET and glass substrates

TCO samples	2θ (deg)		Micro strain (ε) $\times 10^{-2}$		Dislocation density (lines/m^2) $\times 10^{16}$ (δ)		Lattice constant (c) (nm)		Compressive stress (σ) (GPa)	
Substrate	PET	Glass	PET	Glass	PET	Glass	PET	Glass	PET	Glass
Z-1	34.38	34.22	2.09	1.35	2.90	1.20	0.5218	0.5240	−1.04	−2.94
Z-2	34.32	34.12	1.47	1.44	1.43	1.35	0.5227	0.5255	−1.82	−4.24
AZ-1	33.98	33.78	5.43	2.20	19.18	3.11	0.5277	0.5307	−6.14	−8.73
AZ-2	34.06	33.86	3.99	1.91	10.41	2.35	0.5264	0.5295	−5.01	−7.69

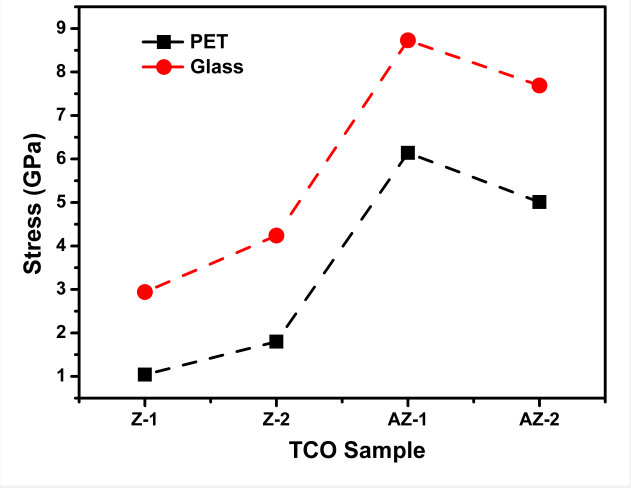

Figure 4 Compressive stress on Z-TCO and AZ-TCO layers deposited on PET and glass substrates.

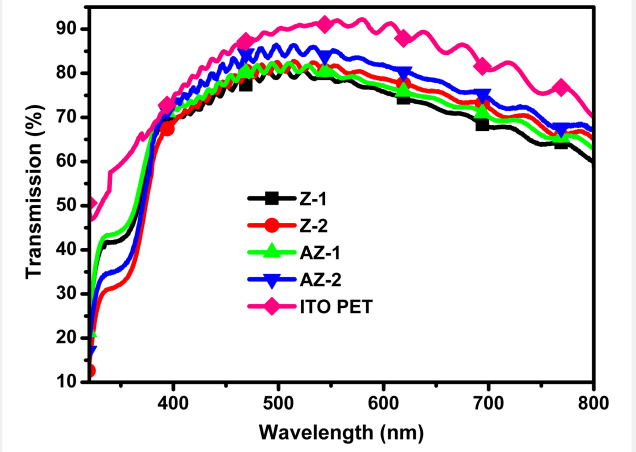

Figure 5 Transmission spectra of Z-TCO and AZ-TCO multilayer films.

that on Z-1 and Z-2 for both PET and glass substrates, which may be due to the incorporation of Al.

Thus, Z-TCO and AZ-TCO layers on the PET substrate show almost similar surface and stress characteristics to those on the glass substrate and should be able to withstand device-processing steps. This makes the Z-TCO and AZ-TCO deposited on the PET substrate a promising candidate to use as a TCO for flexible optoelectronic devices.

The optical transmission spectra of the Z-1 and Z-2, AZ-1, and AZ-2 multilayers along with ITO PET for comparison are shown in Figure 5. All the multilayer TCO samples exhibit sharp transmittance enhancements in the UV region. The average transmittance of Z-TCO and AZ-TCO is ~75–81% in the 400–700 nm region and the transmittance decreases thereafter. The increase of free-carrier absorption results in the reduction of transmittance at the near-IR wavelength region (> 700 nm).[35,36] For Z-1 and Z-2, the average transmittance in 400–700 nm is 75.4% and 77.6%, respectively, whereas for AZ-1 and AZ-2, the average transmittance is 77.0% and 80.8%, respectively.

Expectedly, for both the multilayer structures the transmittance increases for 10 nm Ag thickness. The growth of Ag films of different thicknesses by varying deposition time can influence the optical and electrical characteristics of an RF-deposited TCO film. In the initial stage of deposition, clusters of Ag particles are distributed randomly onto the ZnO or AZO surface, thereby increasing light scattering. With increased Ag deposition, coalescence among Ag particles owing to increased surface diffusion leads to a continuous thin-film formation.[37] This eventually reduced interfacial scattering, which results in an enhancement in optical transparency. The Z-2 and AZ-2 samples show a maximum optical transparency of 82.7% and 86.4%, at 515 and 498 nm, respectively. The optical and electrical characteristics of the RF-deposited Z-TCO and AZ-TCO multilayer TCOs are compared with the properties of ITO PET (Table 4). The electrical parameters of TCO layers were calculated using Hall effect measurement and a four-probe measurement system. Table 4 shows that the electrical resistivity and sheet resistance of the deposited Z-TCO and AZ-TCO layers are much lower than those of ITO PET. Similarly, the carrier concentration of the fabricated TCO layers is higher than the ITO PET film.

This confirms the Ag clusters' agglomeration to form a smooth continuous layer and a reduced surface scattering effect, thereby decreasing the resistivity of the Z-2 and AZ-2 multilayer films. The reduction of sheet resistance of the

Table 4 Electrical and optical parameters of Z-TCO and AZ-TCO multilayers

TCO sample	Resistivity (Ω cm)	Carrier concentration (cm^{-3})	Mobility ($cm^2 \cdot V^{-1} \cdot s^{-1}$)	Sheet resistance (Ω/sq)	FoM (10^{-3} Ω^{-1}) at λ = 400–700 nm
Z-1	4.82×10^{-5}	4.7×10^{21}	27.6	7.1	8.4
Z-2	4.34×10^{-5}	4.5×10^{21}	32.0	6.2	12.9
AZ-1	4.35×10^{-5}	4.1×10^{21}	35.0	6.4	11.5
AZ-2	3.92×10^{-5}	3.9×10^{21}	40.8	5.6	21.3
ITO PET	2.62×10^{-4}	7.3×10^{20}	32.6	14.5	17.3

multilayer at a higher Ag thickness is also attributed to significant increases in available free carriers in the structures.[10,26]

The variation in electrical parameters of the fabricated Z-TCO and AZ-TCO layers is shown in Figures 6 and 7. Both Z-2 and AZ-2 layers expectedly have lower electrical resistivity and sheet resistance compared to Z-1 and AZ-1 layers.

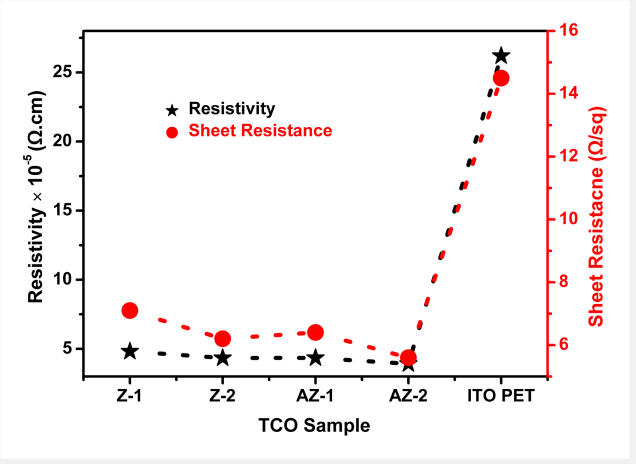

Figure 6 Resistivity and sheet resistance variation for Z-TCO and AZ-TCO layers.

Figure 7 shows the variation of carrier concentration and mobility of the prepared Z-TCO and AZ-TCO layers. For both Z-TCO and AZ-TCO structures, the mobility of the charge carrier is higher for 10 mm Ag thickness, which is attributed to the reduced interface scattering and improved crystallinity as described earlier. Moreover, the decrease in carrier concentrations at higher Ag thicknesses also results in increased mobility.[38]

It can also be observed that the Z-2 and AZ-2 layers display a higher mobility and a lower electrical resistivity compared to the Z-1 and AZ-1 layers. Further, compared to Z-TCO layers, the AZ-TCO layers possess a higher carrier mobility and a lower electrical resistivity. Although the ITO PET exhibits higher mobility than Z-1 and Z-2, AZ-1 and AZ-2 show much higher mobility. Among all the samples, the AZ-2 layer has the highest mobility of 40.8 $cm^2 \cdot V^{-1} \cdot s^{-1}$ and the lowest electrical resistivity of 3.92×10^{-5} Ω cm, while for the ITO PET sample, the mobility is 32.6 $cm^2 \cdot V^{-1} \cdot s^{-1}$ with an electrical resistivity of 2.62×10^{-4} Ω cm. So, the RF-deposited Z-TCO and AZ-TCO multilayer TCOs with an average optical transparency of ~75–81% in the 400–700 nm wavelength region and low electrical resistivity with high mobility are promising replacements of ITO PET films for flexible device fabrication.

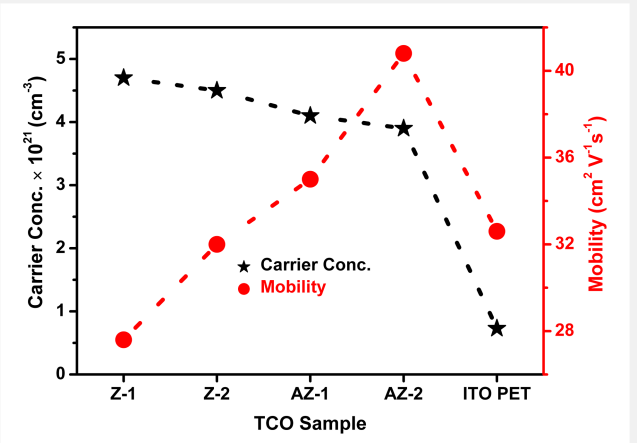

Figure 7 Carrier concentration and mobility variation for Z-TCO and AZ-TCO layers.

The FoMs of the Z-TCO and AZ-TCO layers are calculated using the Haacke equation.[39]

$$\Phi_{TC} = \frac{T^{10}}{R_s} \tag{7}$$

Here, R_s is the sheet resistance and T is the average transmittance.

The FoM for the AZ-2 layer is 21.3×10^{-3} Ω^{-1}, which is higher than that for the ITO PET film (17.3×10^{-3} Ω^{-1}). In order to understand the role of the substrate, the optical and electrical properties of the Z-2, AZ-2, and ITO films on PET substrates are also compared with the properties of Z-2 and AZ-2 on glass substrates, as reported in our previous article.[19] The values for ITO on glass are given for comparison (Table 5). The Z-2 and AZ-2 films on the glass substrate exhibit better optical and electrical properties compared to those on the PET substrate. A higher surface roughness of the top ZnO layer for PET will increase the light scattering, contributing to the decrease in light transmission. Although the sheet resistance of the Z-2 and AZ-2 films on the PET surface is comparable to that on the glass surface, the mobility and FoM for all samples on glass are much higher than those on the PET surface. The higher FoM value for glass is mainly attributed to the higher optical transparency.

Figure 8 shows the band gaps of Z-TCO and AZ-TCO layers calculated from diffuse reflectance using the Kubelka–Munk

Table 5 Comparison of optical and electrical properties of Z-2, AZ-2 and ITO films on glass and PET substrates

TCO sample	Carrier concentration (cm^{-3})		Mobility ($cm^2 \cdot V^{-1} \cdot s^{-1}$)		Sheet resistance (Ω/sq)		FoM (10^{-3} Ω^{-1}) at λ = 400 – 700 nm	
	Glass	PET	Glass	PET	Glass	PET	Glass	PET
Z-2	4.5×10^{21}	4.5×10^{21}	36.7	32.0	5.4	6.2	22.4	12.9
AZ-2	3.6×10^{21}	3.9×10^{21}	46.8	40.8	5.3	5.6	45.5	21.3
ITO	4.1×10^{20}	7.3×10^{20}	33.4	32.6	16.8	14.5	23.7	17.3

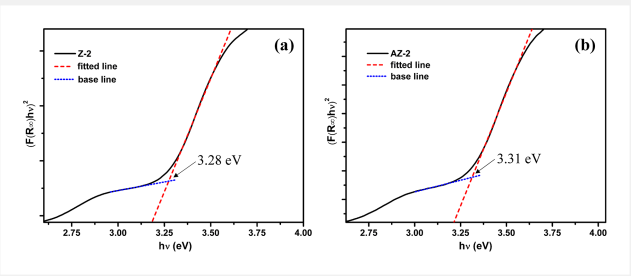

Figure 8 Calculated bandgap of (a) Z-2 and (b) AZ-2 multilayers.

method.[40,41] The band gaps of the fabricated Z-2 and AZ-2 layers are 3.28 to 3.31 eV, respectively (intersection of the fitted line and baseline).

The fabricated Z-TCO and AZ-TCO structures with the band gap above 3.31 eV permit higher light transmission above 350 nm in the visible region and are obviously well suitable as TCOs for optoelectronic devices. Thus, Z-TCO and AZ-TCO structures having excellent FoMs can be a cheaper option for using as TCOs for flexible optoelectronic devices.

Conclusions

The preparation of highly transparent, conducting Z-TCO and AZ-TCO multilayer TCOs on flexible PET using an RF magnetron sputtering system is reported. The thicknesses of these Z-TCO and AZ-TCO multilayer films are about 70 nm. Compressive stress dominates the surface behaviour of top ZnO thin films for both PET and glass substrates. The Z-TCO and AZ-TCO layers on the PET substrate show almost similar surface characteristics to those on the glass substrate, with surface roughness of ~5 – 7 nm on PET substrates being within the required range for any device applications. These sputtered deposited flexible Z-TCO and AZ-TCO layers possess excellent optical and electrical properties. The average transmittance of these TCO samples is around ~75 – 81% in the 400 – 700 nm wavelength region. Z-2 and AZ-2 TCO layers show improvement in crystallization with reduced sheet resistance and enhanced optical transparency. The AZ-2 layer with thickness AZO (30 nm) + Ag (10 nm) + AZO (30 nm) is found to have superior electrical properties compared to the ITO PET film. The AZ-2 layer has an excellent FoM (21.3×10^{-3} Ω^{-1}) as compared to the ITO PET FoM (17.3×10^{-3} Ω^{-1}). Therefore, these multilayer TCO layers on PET can play an important role in the replacement of the expensive ITO for flexible optoelectronic devices such as solar cells, light-emitting diodes, and other wearable devices.

Experimental Section

Z-TCO and AZ-TCO multilayer films were sequentially deposited by an RF magnetron sputtering system on PET substrates using a zinc oxide (ZnO) target (99.999 wt.%), a silver (Ag) target (99.99 wt.%), and an aluminium-doped zinc oxide (AZO) target (98 wt.% ZnO and 2 wt.% Al_2O_3), each of 4 inch in diameter. Successive depositions of ZnO, AZO, and Ag layers were done at ambient temperature by using a substrate-moving arm, installed in the multitarget sputtering system. The deposition parameters and thickness of each layer of ZnO, AZO, and Ag on PET substrates are the same as on glass substrates reported in our previous article.[19] Before loading into the chamber of the sputtering system, all the flexible substrates were ultrasonically cleaned for 15 min separately in ethanol and deionized water in an ultra-sonicator. The ultrasonically cleaned substrates were dried with N_2. Before deposition on the substrate, ZnO, Ag, and AZO targets were subjected to pre-sputtering for 15 min to avoid contamination. More details about the deposition of multilayer TCO and characterization techniques are available in the Supporting Information.

Funding Information

The work presented in this research article was done under the Department of Science and Technology (DST) – Research Council UK (RCUK) project "SUNRISE."

Acknowledgment

S.K.S. thanks the Department of Science and Technology, New Delhi, India for an INSPIRE Faculty Award. The authors are also thankful to Nanoscale Research Facility (NRF) and Central Research Facility (CRF), IIT Delhi for the characterization facilities.

Supporting Information

Supporting Information for this article is available online at https://doi.org/10.1055/s-0042-1757982.

Conflict of Interest

The authors declare no conflict of interest.

References

(1) Zhang, C.; Ji, C.; Park, Y. B.; Guo, L. J. *Adv. Opt. Mater.* **2020**, *2001298*, 1.
(2) Yang, Y.; Song, W.; Ding, L. *Sci. Bull.* **2020**, *65*, 1324.
(3) Cui, J.; Wang, A.; Edleman, N. L.; Ni, J.; Lee, P.; Armstrong, N. R.; Marks, T. J. *Adv. Mater.* **2001**, *13*, 1476.
(4) Kumar, A.; Zhou, C. *ACS Nano* **2010**, *4*, 11.
(5) Swami, S. K.; Chaturvedi, N.; Kumar, A.; Dutta, V. *Mater. Today Energy* **2018**, *9*, 377.
(6) Swami, S. K.; Chaturvedi, N.; Kumar, A.; Dutta, V. *Prog. Photovoltaics Res. Appl.* **2016**, *24*, 74.
(7) Zhang, S. X.; Dhar, S.; Yu, W.; Xu, H.; Ogale, S. B.; Venkatesan, T. *Appl. Phys. Lett.* **2007**, *91*, 112113.
(8) Cho, K. S.; Kim, H. K. *RSC Adv.* **2018**, *8*, 2599.
(9) Wu, H. W.; Yang, R. Y.; Hsiung, C. M.; Chu, C. H. *J. Mater. Sci.: Mater. Electron.* **2013**, *24*, 166.
(10) Sivaramakrishnan, K.; Theodore, N. D.; Moulder, J. F.; Alford, T. L. *J. Appl. Phys.* **2009**, *106*, 063510.
(11) Kim, J. H.; Lee, J. H.; Kim, S. W.; Yoo, Y. Z.; Seong, T. Y. *Ceram. Int.* **2015**, *41*, 7146.
(12) Guo, X.; Liu, X.; Lin, F.; Li, H.; Fan, Y.; Zhang, N. *Sci. Rep.* **2015**, *5*, 10569.
(13) Sharma, V.; Kumar, P.; Kumar, A.; Surbhi; Asokan, K.; Sachdev, K. *Sol. Energy Mater. Sol. Cells* **2017**, *169*, 122.
(14) Minami, T. *Semicond. Sci. Technol.* **2005**, *20*, S35.
(15) Girtan, M. *Sol. Energy Mater. Sol. Cells* **2012**, *100*, 153.
(16) Han, H.; Theodore, N. D.; Alford, T. L. *J. Appl. Phys.* **2008**, *103*, 013708.
(17) Guillén, C.; Herrero, J. *Phys. Status Solidi A* **2010**, *207*, 1563.
(18) Fahland, M.; Vogt, T.; Schoenberger, W.; Schiller. N. *Thin Solid Films* **2008**, *516*, 5777.
(19) Barman, B.; Swami, S. K.; Dutta, V. *Mater. Sci. Semicond. Process.* **2021**, *129*, 105801.
(20) Rayerfrancis, A.; Bhargav, B. P.; Ahmed, N.; Balaji, C.; Kumar, G. *EPJ Appl. Phys.* **2018**, *82*, 1.
(21) Swami, S. K.; Chaturvedi, N.; Kumar, A.; Kumar, V.; Garg, A.; Dutta, V. *Sol. Energy* **2022**, *231*, 458.
(22) Jayababu, N.; Poloju, M.; Shruthi, J.; Reddy M. V. R. *Mater. Sci. Semicond. Process.* **2019**, *102*, 104591.
(23) Zak, A. K; Razali R.; Mazid, W. H. A.; Darroudi, M. *Int. J. Nanomed.* **2011**, *6*, 1399.
(24) Arefi, M. R.; Rezaei-Zarchi, S. *Int. J. Mol. Sci.* **2012**, *13*, 4340.
(25) Sahu, D. R.; Chen, C. Y.; Lin, S. Y.; Huang, J. L. *Thin Solid Films* **2006**, *515*, 932.
(26) Nezhad, E. H.; Haratizadeh, H.; Kari, B. M. *Ceram. Int.* **2019**, *45*, 9950.
(27) Lu, J. G.; Ye, Z. Z.; Zeng, Y. J.; Zhu, L. P.; Wang, L.; Yuan, J.; Zhao, B. H.; Liang, Q. L. *J. Appl. Phys.* **2006**, *100*, 073714.
(28) Liu, Y.; Li, Y.; Zeng, H. *J. Nanomater.* **2013**, *2013*, 196521.
(29) Song, S.; Yang, T.; Lv, M.; Li, Y.; Xin, Y.; Jiang, L.; Wu, Z.; Han, S. *Vacuum* **2010**, *85*, 39.
(30) Ungar, T.; Gubicza, J.; Ribárik, G.; Borbély, A. *J. Appl. Crystallogr.* **2001**, *34*, 298.
(31) Jazmati, A. K.; Abdallah, B. *Mater. Res.* **2018**, *21*, 1.
(32) Motevalizadeh, L.; Heidary, Z.; Abrishami, M. E. *Bull. Mater. Sci.* **2014**, *37*, 397.
(33) Riascos, H.; Orozco, S.; Uzuriaga, J. *Procedia Mat. Sci.* **2015**, *9*, 523.
(34) Abadias, G.; Chason, E.; Keckes, J.; Sebastiani, M.; Thompson, G. B.; Barthel, E.; Doll, G. L.; Murray, C. E.; Stoessel, C. H.; Martinu, L. *J. Vac. Sci. Technol., A* **2018**, *36*, 020801.
(35) Giovannetti, F.; Föste, S.; Ehrmann, N.; Rockendorf, G. *Sol. Energy* **2014**, *104*, 52.
(36) Szczyrbowski, J.; Dietrich, A.; Hartig, K. *Sol. Energy Mater.* **1987**, *16*, 103.
(37) Mohamed, S. H. *J. Phys. Chem. Solids* **2008**, *69*, 2378.
(38) Li, R.; Zhou, Y.; Sun, M.; Gong, Z.; Guo, Y.; Wu, F.; Li, W.; Ding, W. *Coatings* **2019**, *9*, 591.
(39) Haacke, G. *J. Appl. Phys.* **1976**, *47*, 4086.
(40) Makuła, P.; Pacia, M.; Macyk, W. *J. Phys. Chem. Lett.* **2018**, *9*, 6814.
(41) Kubelka, P.; Munk, F. A. *Z. Tech. Phys.* **1931**, *12*, 593.